11

Electrochemical Spark Micromachining Process

Anjali Vishwas Kulkarni
Centre for Mechatronics, Indian Institute of Technology Kanpur, India

1. Introduction

Electrochemical spark micromachining process (ECSMM) is a process suitable for micromachining of electrically non-conducting materials. Besides the classic semiconductor technology, there are various methods and processes for micromachining such as Reactive Ion Etching (RIE) (Rodriguez et al., 2003), femto-second pulse laser radiation (Hantovsky et al., 2006), chemical etching and plasma-enhanced chemical vapor deposition (Claire, 2004)], spark assisted chemical engraving (Fasico and Wuthrich, 2004) and micro-stereo-lithography (Rajaraman, 2006) in practice. Use of photoresist as sacrificial layer to realize micro-channels in micro fluidic systems is discussed in (Coraci, 2005). All these methods are expensive as they need the vacuum, clean environment and mostly involve in between multi processing steps to arrive at the final microchannel machining results. There is a need of an innovative process which is cost effective and straight forward without employing intermediate processing steps. One such process thought of and being researched is electrochemical spark micromachining (ECSMM) process. The ECSMM process is a stand alone process unlike others and it does not demand on intermediate processing steps such as: masking, pattern transfer, passivation, sample preparation etc. The use of separate coolants is also not required in performing the micromachining by ECSMM.

Micromachining needs are forcing reconsideration of electrochemical techniques as a viable solution (Marc Madau, 1997). Another similar process termed as spark assisted chemical engraving (SACE) (Wuthrich et al., 1999) has been employed for the micromachining of glass. ECSMM is a strong candidate for microfabrication utilizing the best of electrochemical machining (ECM) and electro discharge machining (EDM) together. Applications of ECS for microfabrication can be in the field of aeronautics, mechanical, electrical engineering and similar others. It can successfully process silicon (Kulkarni et. al., 2010a), molybdenum (Kulkarni et. al., 2011c), tantalum (Kulkarni et. al., 2011a), quartz (Deepshikha, 2007; Kulkarni et. al., 2011a), glass ((Kulkarni et al., 2011a, 2011b); Wuthrich et al. 1999)), alumina (Jain et al., 1999), advanced ceramics (Sorkhel et al., 1996) and many other materials.

The chapter discusses the details of the experimental set-up developed in the next section. The procedure for micromachining using the developed set-up is outlined next. The experimental scheme to perform machining on glass pellets (cover slips used in biological applications) is presented. Discussion of the micro machined samples is presented. This discussion is based on various on line and post process measurements performed. The qualitative material removal mechanism is presented based on the results and discussions.

2. Experimental set-up

A functional set-up of the ECSMM process is designed, developed and fabricated as shown in Figure 1 (Kulkarni et. al., 2011b). The main components of the ECS set-up are as follows and are described in the following sub sections:

1. Machining Chamber
2. Power Supply System
3. Exhaust System
4. Control PC

2.1 Machining chamber

The machining chamber houses X-Y table, Z axis assembly, tool feed and tool holder assembly and ECS cell. X, Y, Z and tool feed stages are motorized.

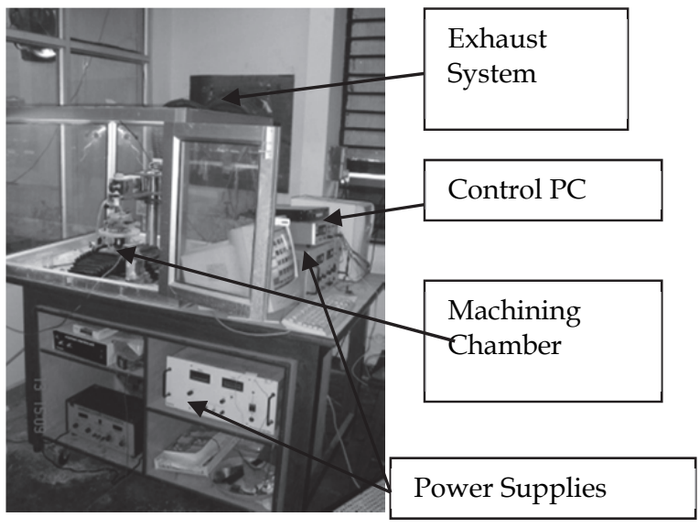

Fig. 1. Photograph of experimental set-up (Kulkarni et al., 2011b)

2.1.1 X-Y table

X-Y table has resolution of 2 µm in X and Y directions and traverse of 100 mm in X as well as Y directions. The guide ways use non-recirculating balls as rolling elements. The mechanical drive is a ground lead screw of 400 µm pitch made of aluminium alloy. Rotation to the X and Y screws is provided by separate stepper motors. The table is mounted on a chrome plated MS plate. Chrome plating protects the plate from corrosion. The MS plate has mounting tapped holes on a 25 mm grid to mount the ECS cell. Bellows are provided to protect the motors and lead screws from the electrolyte splashes and fumes produced.

2.1.2 Z axis assembly

The Z axis is automated to move up or down to maintain a constant work piece-tool gap. The worm and worm wheel with a gear ratio of 1:38 transmit the power to a lead screw of 200 µm pitch. All the parts are fabricated with stainless steel and brass to resist corrosion due to acidic environment. It has positioning accuracy of 50 µm and maximum vertical travel of 80 mm.

2.1.3 Tool feed and tool holder assembly

Tool feed assembly is mounted on Z axis assembly. A glass tool holder is designed and developed. This tool holder provided the tool insulation and hence reduction in the stray currents. This glass tool holder is used to hold the tool wire in place. A fixture made of Perspex material is designed and fabricated to hold the tool holder on Z assembly. Cu wire of 200 µm diameter is used as a cathode (tool).

2.1.4 ECS cell

It is a rectangular box of 10 cm x 8 cm x 6 cm dimensions made up of Perspex material. It is mounted on X-Y table. It houses separate fixture arrangement for graphite anode and work piece holder. It is filled with the electrolyte. The electrolyte level is maintained at 1mm above the flat surface of the work piece. Electrolyte used is NaOH in varied concentration in the range of 14-20 %.

2.2 Power supply system

DC regulated power supplies of different ratings are used for driving stepper motors, machining supply and control circuitry. Use of separate power supply ensures the noise free operation.

2.3 Exhaust system

Proper exhaust system is designed and provided to take away the electrolyte fumes generated during the spark process inside the machining chamber. A small DC operated fan is placed in the machining chamber where the fumes are generated. These are carried away by a hose pipe and thrown away from the room with an exhaust fan.

2.4 Control PC

Stepper motors used for driving X, Y, Z and tool feed are all interfaced to motion controller card installed in PC. Precise control and drive of the machine is achieved with NI 7834 PCI card and NI 7604 drive board interfaced to a computer. Contouring functions in LabVIEW platform are used to carve different shapes of the micro channels [Kulkarni et al., 2008].

3. Experimental procedures

The supply voltage, electrolyte concentration and table speed are the control parameters. Pilot experiments are performed to determine the optimum window of these operating parameters.

It is observed that sparking occurs at supply voltage of 30 V and above. Glass samples break above 50 V supply voltage. Hence the working supply voltage range chosen is 40 V – 50 V.

Use of base solution is preferred over the acidic electrolyte. It was observed that in the acidic environment the surface roughness increases. The fumes formed of acidic solutions during the electrochemical sparking process are harmful. During the pilot experiments it was observed that machining takes place in diluted sodium hydroxide (NaOH) solution as electrolyte. The concentration window was decided upon by performing many experiments to arrive at a permissible concentration range. It was observed that machining does not take place below 14% concentration of NaOH. Above 20 % concentration of NaOH, the machined surface roughness is notable. Hence 14% -20% concentration range for NaOH electrolyte is

arrived at. Moreover use of low concentration of NaOH as electrolyte makes the ECSMM process as a 'green process'. Level of electrolyte is maintained at 1 mm above the work piece surface in the ECS cell.

The table speed is chosen ranging between 12.5 µm/s – 25 µm/s. It is such that the traverse is not too slow to dig the micro channel and not too fast to miss the micro machining in that region.

Micro channels are formed using the ECSMM process on microscopic glass pellets using platinum wire as a tool of 500 µm diameter. Pellets are of 180 µm thickness, 18 mm diameter circles in size. Length of the tool protruding out of the tool holder is 4 mm. The gap between the cathode tool electrode tip and the work piece surface is maintained at around 20 µm using the tool feed device mounted on Z-axis. The distance between the tool and the anode is 40 mm. Figure 2 shows the photograph of the electrolytic cell with the spark visible at tool tip and electrolyte interface. Graphite anode is seen in the cell. It is a non consuming electrode.

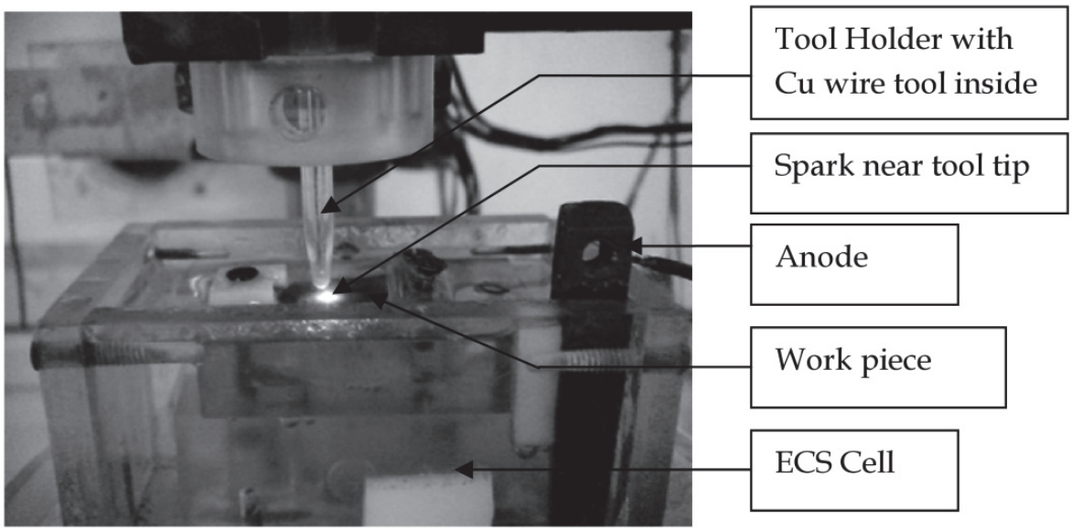

Fig. 2. Photograph of the ECSMM cell with graphite anode, tool and work piece. The spark is visible near the tool tip (Kulkarni et al., 2011b).

Experiments are conducted with Voltage, Electrolyte Concentration and Table Speed as the control variables. The experiments are conducted in accordance with the central composite design scheme developed by the software 'Design Expert 07' to study the response surface. The range of the control variables chosen is as shown below:

- Factor 1 (V_s): Supply voltage ranging between 40 V - 50 V
- Factor 2 (EC): Electrolyte Concentration (NaOH) ranging between 14% - 20%
- Factor 3 (TS): Work piece Table Speed ranging between 12.5 µm/s – 25 µm/s

The design resulted in total of twenty one experiments, out of these twenty one experiments, six central experiments were performed at 45 V supply voltage, 17 % electrolyte concentration and 18.75 µm/s table speed as the values for the control variables.

The responses measured are: average process current (I), width of microchannel (W) and depth of microchannel (D) formed using ECSMM. The scheme of the experiments is as shown in Table 1. Columns 2-4 list V_s, EC, and TS respectively. Columns 5-7 give average current, width, and depth of the microchannels respectively as the responses measured post process.

	Control Variables			Responses			Comments
R #	V_s (V)	EC (%)	TS (µm/s)	I (A)	W (µm)	D (µm)	Channel Type
1	45	17	18.75	0.05	760.5	-	Through
2	40	14	25	0.025	520	-	Through
3	50	14	12.5	0.105	450	-	Through
4	45	17	18.75	0.105	580	-	Through
5	45	17	18.75	0.12	790.5	-	Through
6	45	17	30	0.09	1030	-	Through
7	**36.6**	**17**	**18.75**	**0.06**	**421.5**	**81.5**	**Blind**
8	**40**	**20**	**25**	**0.08**	**870**	*	**Blind**
9	50	20	12.5	0.015	1110	-	Through
10	50	20	25	0.0933	1090	-	Through
11	**40**	**20**	**12.5**	**0.205**	**720.5**	*	**Blind**
12	**45**	**17**	**18.75**	**0.115**	**970.5**	**97.5**	**Blind**
13	**45**	**17**	**18.75**	**0.966**	**1030**	**97.5**	**Blind**
14	40	14	12.5	0.025	585	-	Through
15	50	14	25	0.0733	600	-	Through
16	**45**	**17**	**18.75**	**0.5**	**855**	**97.5**	**Blind**
17	**53.4**	**17**	**18.75**	**2.493**	**610**	**81.5**	**Blind**
18	**45**	**11.9**	**18.75**	**0.6**	**480**	**77.25**	**Blind**
19	45	11.9	18.75	0.05	560	-	Through
20	**45**	**22**	**18.75**	**0.08**	**485.5**	**123.6**	**Blind**
21	45	17	8.45	0.16	810	-	Through

(* could not be measured)

Table 1. Experimental parameters and responses

3.1 On line measurements

The average process current is measured with the help of a digital multimeter. Besides this average current, the time varying process current is measured on line by digital storage oscilloscope. For this purpose the 'resistive shunt method' is used. In this a 1 Ω resistance is connected in series with cathode and ground of the power supply to the ECS cell. The time varying voltage across this resistance is the direct measure of the time varying process current. The wave forms are saved on the control PC via RS 232 connectivity module of the oscilloscope (Hameg 1008). The on-time, off-time and the frequency of the sparks occurring are measured. These parameters are otherwise theoretically estimated. The occurrences of these pulses directly indicate the correlation between the presences of the sparks during the process. The analysis of these current pulses will be helpful to devise the electrical model of the process.

3.2 Post process measurements

A set-up is developed to measure the depth of the microchannels at various points with the resolution of 10 µm. The dial gauge used for this purpose is mounted on the Z Axis of a standard machine to achieve these measurements.

To study the surface topography and width measurement, SEM analysis of the micro channels is performed. SEM at different and higher magnification is performed to get the insight into the surface topography due to this process. SEM at increasing magnification clearly shows the imprints and development of how the material is removed from the work piece surface.

The results based on the above studies are presented in the following section.

4. Results and discussions

Measurements of on line average current, and post measurements of width and depth of microchannels are presented in Table 1 in column 5-7. Theses are discussed in details in the following sub sections. To study the surface topography and width measurement, SEM analysis of the microchannels is performed. Following section describes the microstructure analysis of the microchannels.

4.1 Microstructure Analysis by SEM

Detailed SEM is performed for the samples of central experiments (at 45 V, 17% electrolyte concentration, and 18.75 μm/s table speed) to study the effect of sparking on the microstructure. SEM is performed at successive higher magnification to visualize the surface closely. Figure 3 shows the photograph of three microchannels (forming an inverted 'C' section) carved at 45 V, 17% electrolyte concentration and 18.75 μm/s table speed. These are formed using X traverse through 2500 pulses in carving channel 1, Y traverse in carving channel 2 and then negative X traverse of X-Y table in carving the third channel, i.e. channel 3. The length of each section in the C type micro channel is about 5000 μm. The average width of channel 2 is around 535 μm and the average depth is around 370 μm.

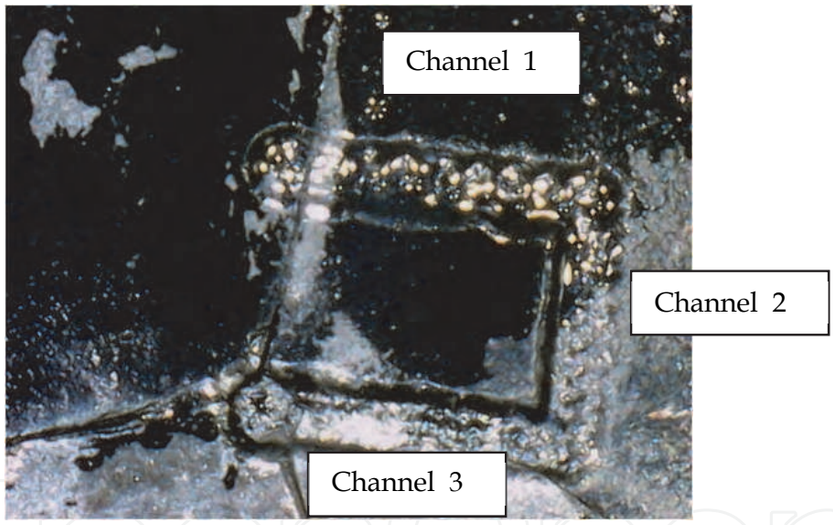

Fig. 3. USB Photograph of the channels carved at 45 V, 17% electrolyte concentration and 18.75 μm/s table speed. The approximate length of each channel is 5000 μm, average width is 535 μm, and depth is 370 μm.

Figure 4 gives the microstructure of the micromachined glass surface at 162 X magnification carved at 37 V, 17% electrolyte concentration and 18.75 μm/s table speed. From SEM picture it is obvious that a shallow microchannel is obtained. This may be due to the lower supply voltage of 37 V. The width at two different regions of microchannel is 267 μm and 410.3 μm. Thus, average width of microchannel is 338.65 μm.

Figure 5 gives the microstructure of the micromachined coverslip surface at 881X magnification.The microstructure clearly shows the removal of material along the path of tool movement. Valleys and ridges are clearly visible which are due to melting and the layer by layer material removal in the spark affected region. A piece of material is seen which got re solidified and remained there.

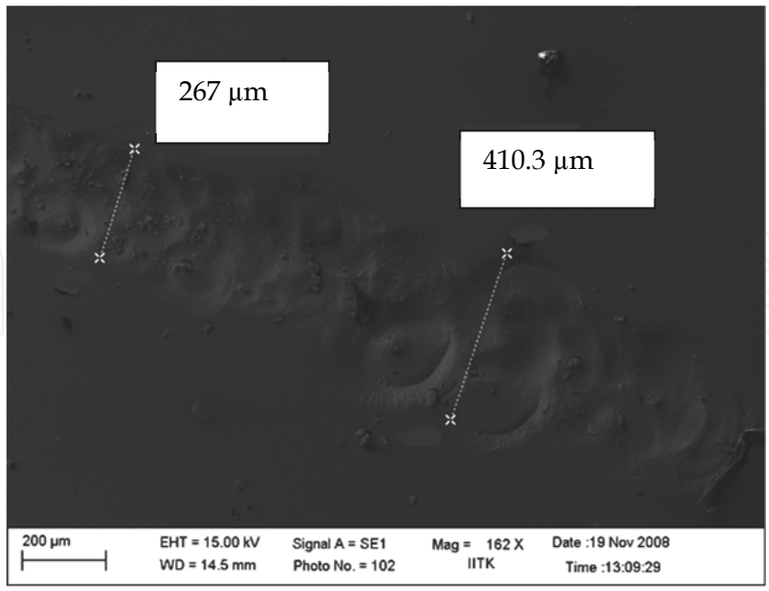

Fig. 4. SEM image (162X) showing width at two places along the microchannel, the average width of the channel is around 338.65 µm at 37 V, 17% electrolyte concentration and 18.75 µm/s table speed.

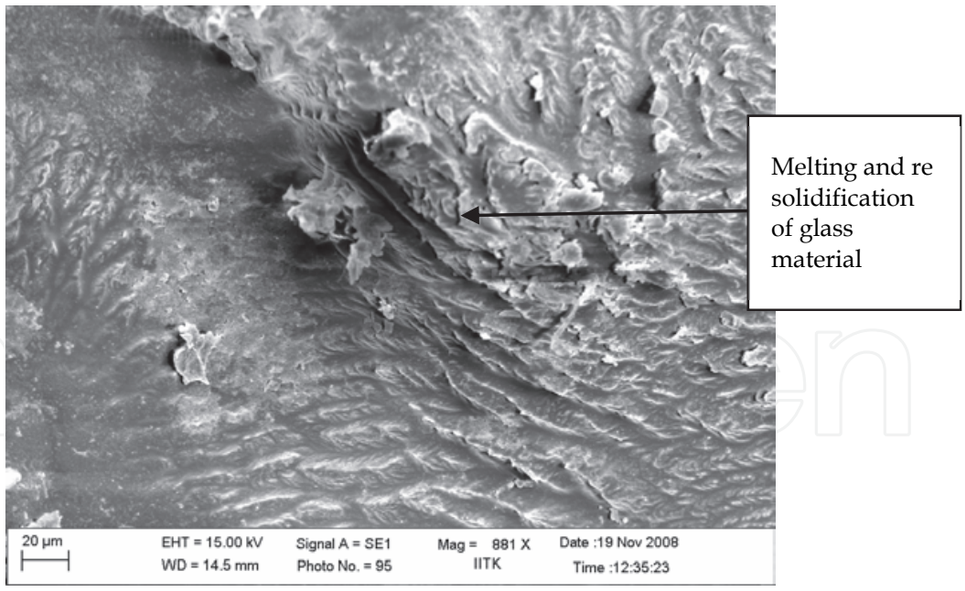

Fig. 5. SEM image of pellet (881X) treated at 45 V, 12% electrolyte concentration and 18.75 µm/s table speed.

Figure 6 gives the microstructure of the microchannel at 4500X magnification. The tearing off of the material is seen. The region shows the melting and solidification of the workpiece material. The thickness of the smallest layer at the corner is around 7.8 µm.

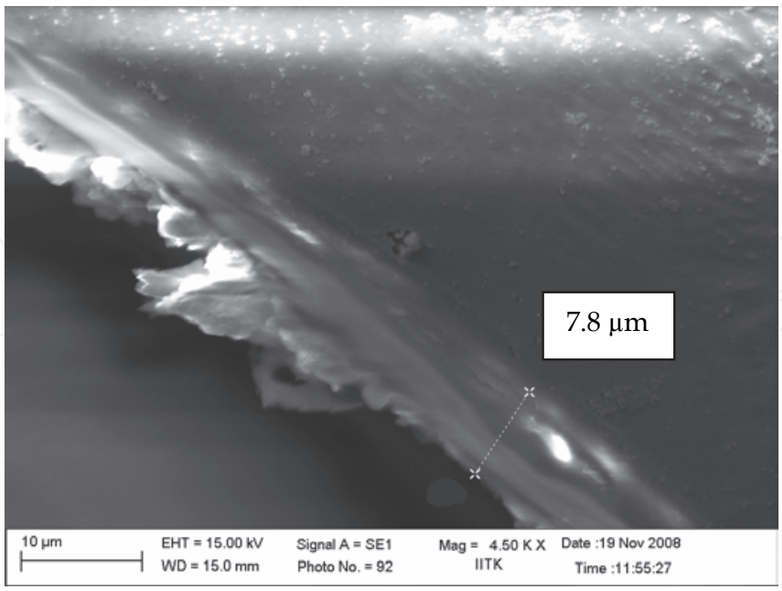

Fig. 6. SEM image (4500X) giving thickness of layer at the corner around 7.8 µm at 45 V, 17% electrolyte concentration and 18.75 µm/s table speed.

4.2 Current analysis

4.2.1 On line average process current

Column 5 of Table 1 gives the values of the average process current measured on line. The electro chemical action causing the migration of ions, and electrons contributes to the average current. The average current value as seen in Table 1, column 5 is ranging from 0.0125 – 0.9 A. Occasionally it has shoot up to 2.493 A for R#17 for 53.4 V supply voltage.

The interesting process phenomenon is not obvious from only recording the average current. The processes' time varying nature can be only revealed by studying the transient current. The transient current waveforms reveal the process complexity and help in understanding the holistic and time changing phenomena during the single entire current cycle of ECSMM process, as explained in the next section. The actual machining is occurring during the very short time of the instantaneous current pulses carrying high energy density.

4.2.2 On line, transient process current

The time varying current is measured with the help of a digital storage oscilloscope as mentioned in section 3.1. The snap shots of the stored waveform are presented in Figures 7 a and b. In Figure 7a it can be noted that there are many spikes during a time of 10 ms duration corresponding to 1 division of oscilloscope window. Each pulse represents a spark occurrence. The average process current can be seen at a level of 0.1 A. A pulse of height of 0.3 A can be seen of time period greater than 20 ms. A second pulse of instantaneous current value more than 0.4 A can be seen after a period of around 15 ms. It's time period is about 6ms. Many short duration (<1ms) pulses can be seen in between these two remarkable pulses. These pulses show the stochastic nature of the spark formation process.

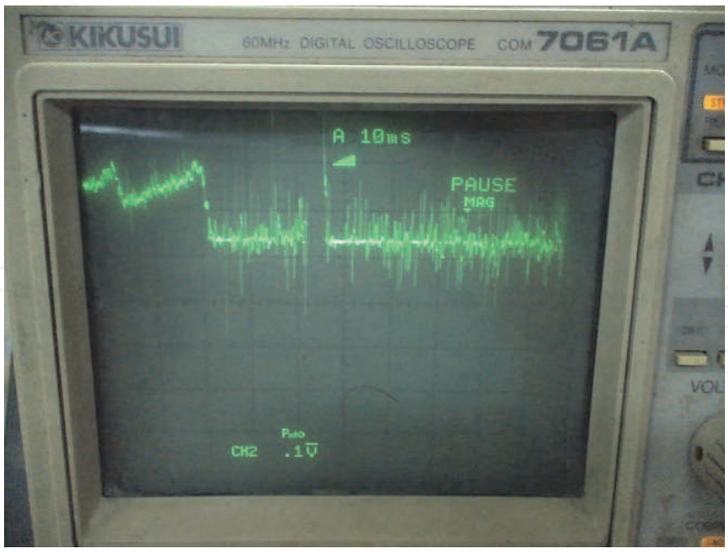

Fig. 7 a. Snap shot of online time varying ECSMM process current during glass pellet micromachining.

In another waveform, Figure 7 b, two complete current pulses and two halfway current pulses can be seen. These are of different time durations, ranging from 0.1 ms to 0.3 ms time period. Hence the resulting frequency is variable and is ranging from 2.5 kHz to 5 kHz. The sparking frequency depends on many factors such as size of bubble formed, bubble growth time, time of its survival, etc. The size of the spark or discharge depends on the instantaneous current value. It is clear from these time varying current pulses that sparks of different energy strike the work piece surface resulting in softening, melting, and / or vaporizing of the work piece material.

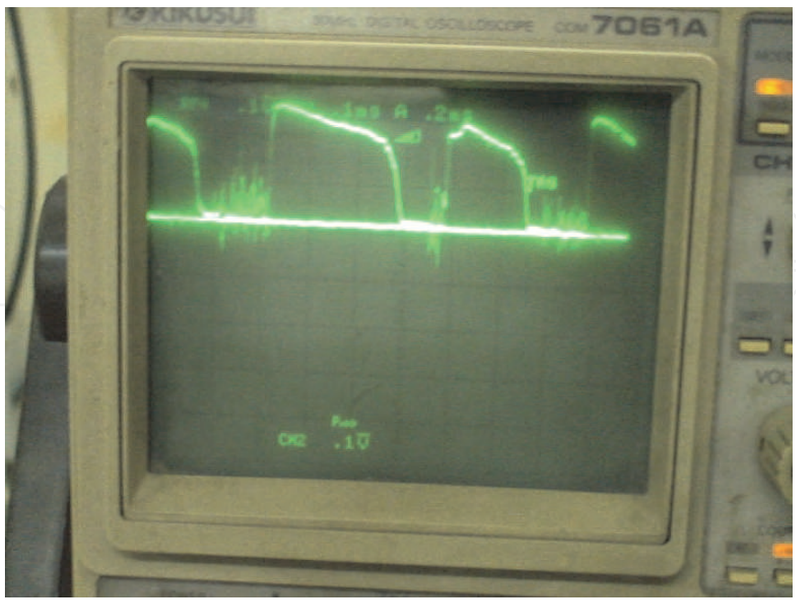

Fig. 7 b. Snap shot of online time varying ECSMM process current during glass pellet micromachining.

The spark energy can be estimated by taking V_s = 45 V, $i_{instantaneous}$ = 0.2 A and time = 0.2 ms. The instantaneous spark energy with a striking area of diameter less than the tool diameter, i.e. 200 μm, is of the order of 500 kJ/m^2.

4.3 Width of microchannels

Columns 6 of Table 1 gives post process measured values of the width of the microchannels using the dial gauge. The last column summarizes the type of the microchannel formed. It says whether a channel is a through channel or a blind microchannel achieved. The rows corresponding to the successfully achieved microchannels are shown in bold face. The depth of the microchannels in Run # 8 and # 11 could not be measured for some reasons. In case of the through channels the depth of the microchannel achieved is more than 180 μm. Either the higher machining time or the lower travel speed or the smaller gap due to local irregularities is responsible for through machining to occur.

The minimum width achieved is 421.5μm for Run # 7 for 36.6 V, 17 % electrolyte concentration and 18.75 μm/s table speed. The maximum width achieved is 1110 μm for Run # 9 for 50 V, 20 % electrolyte concentration and 12.5 μm/s table speed. That means for higher voltage, higher electrolyte concentration and lower table speed combination of parameters, the width achieved is higher.

4.4 Depth of microchannels

The minimum depth achieved is 77.25 μm for Run # 18 for 45 V, 11.9 % electrolyte concentration and 18.75 μm/sec table speed. The maximum depth achieved is 123.6 μm for Run # 20 for 45 V, 22 % electrolyte concentration and 18.75 μm/sec table speed. Higher electrolyte concentration results in higher depth. Microchannels of the width between 400 – 1100 μm are achieved. The depth achieved is 75 -120 μm.

For other experiments, through machining has been occurred where the depth of cut is more than the thickness of the work piece. This may be partly due to the gap adjustment between the tool and the work piece surface. It is a crucial operation to maintain the gap at or above 20 μm without the closed loop control. This calls for a close loop control for maintaining the gap between the tool and the work piece surface.

A novel technique to measure the depth of these microchannels is devised and discussed in Kulkarni et. al., (2010b) and Kulkarni et. al., (2010c).

Parametric models pertaining to the average current, width and depth of the microchannels' are presented elsewhere.

Section 5 describes the systematic description on understanding the ECSMM process mechanism in view of the transient current.

5. Understanding the process mechanism

The material removal mechanism in ECSMM is complex as it is revealed by the SEM and current pulses analysis in the previous sections. This is primarily due to the non-thermal nature of these sparks. In the existent literature the spark energy is considered to be of thermal nature and thermal analysis and material removal are considered to be due to this thermal source (Jain et al.,1999; Basak & Ghosh, 1992). Experimentally it has been found that the spark is a non thermal discharge. This has been confirmed (Kulkarni et al, 2009) while making an attempt to measure the spark temperature by a pyrometer. Pyrometer failed to

measure the temperature as the radiation is a non thermal type. Instead it is a discharge process similar to that of the breakdown of the hydrogen gas bubble isolating the tool tip from the surrounding electrolyte.

Secondly, electro chemical systems are known to exhibit complex non-linear behavior. These nonlinearities arise due to electro hydro dynamism, ionic reactions, bubble generation, their growth and their breakdown phenomena. The overall process seems to be discrete in nature though the supply voltage is DC. Positive as well as negative spikes are also observed in the current waveforms. The electrochemical kinetics includes negative faradic impedance in the electrolyte solution. There are many intermittent, small amplitude current spikes, of smaller duration. These seem to be representing the partial sparks due to the break down of the small hydrogen bubbles. The partial discharge is due to the total isolation of single or many such bubbles completely isolating the electrolyte contact. On the other place the total or complete sparking is that occurring due to the complete isolation of the cathode tip from the electrolyte surface. This can be understood by the pictorial representation as in Figure 8 a and b. In Figure 8 a, there is a local isolation of the tool tip from the surrounding electrolyte due to a small hydrogen bubble. This causes an instantaneous sparking across the bubble, resulting in a small amplitude current spike. Where as, in Figure 8 b, the tool tip is surrounded by a single larger bubble. Many small sized bubbles coalesce in a single larger bubble resulting in complete isolation of the tool tip from the electrolyte. The sparking resulting due to this kind of total isolation will result in the intensive sparking manifesting the large amplitude current spikes. This kind of behavior is reflected in the nature of the on line time varying current pulses studied. It was observed that the frequency of sparking

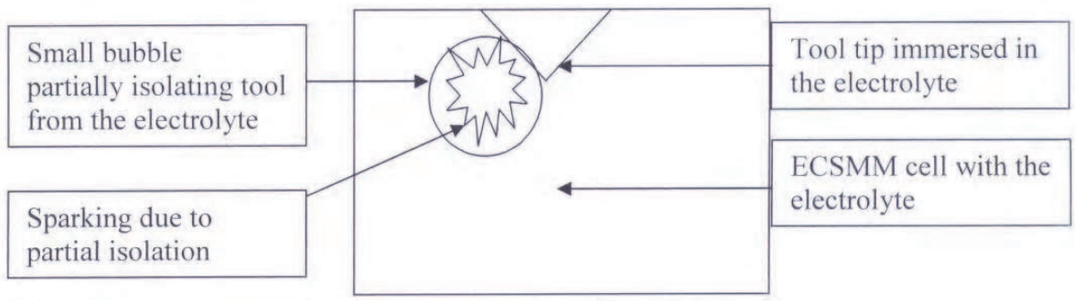

Fig. 8a. Partial sparking due to local isolation by small bubble resulting in a low energy spark

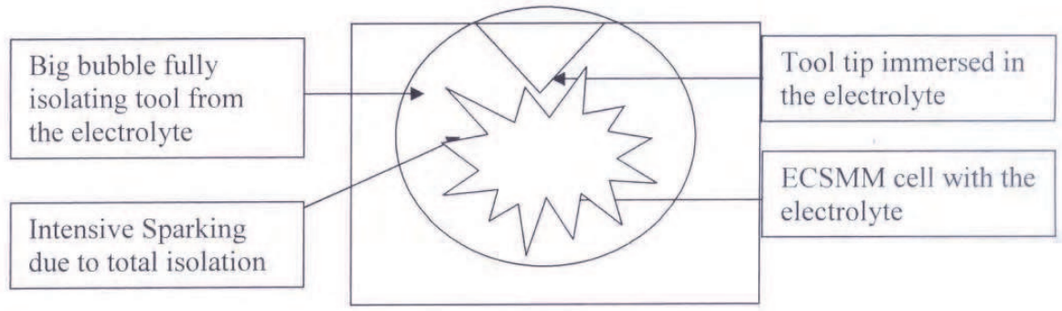

Fig. 8b. Intensive sparking due to complete blanketing of the tool tip by large sized bubble resulting in high energy spark

(oscillations) varies with varying supply voltage (Kulkarni, 2000). The sparking frequency is high (in the tens of MHZ range) and it lowers (in the few hundreds of kHz range) for higher supply voltage. This supports the possibilities of the many partial sparks due to breakdown of the single isolated hydrogen gas bubbles. Theses partial sparks or discharges are of less current value and hence having less energy. These may not result in material removal from the workpiece. These may die out before reaching the workpiece surface.

5.1 Intermediate processes and their interrelation

Thus ECSMM process comprises of many intermediate processes such as electro chemical action causing the migration of ions, followed by the nucleate pool boiling of hydrogen gas bubble due to immense local heating of tool tip immersed in electrolyte. The gas bubble growth dynamics is a complicated phenomenon. It is changing the isolation between the cathode tip from the electrolyte and hence creating a varying electric field. This varying electric field in turn affects the bubble growth dynamics.

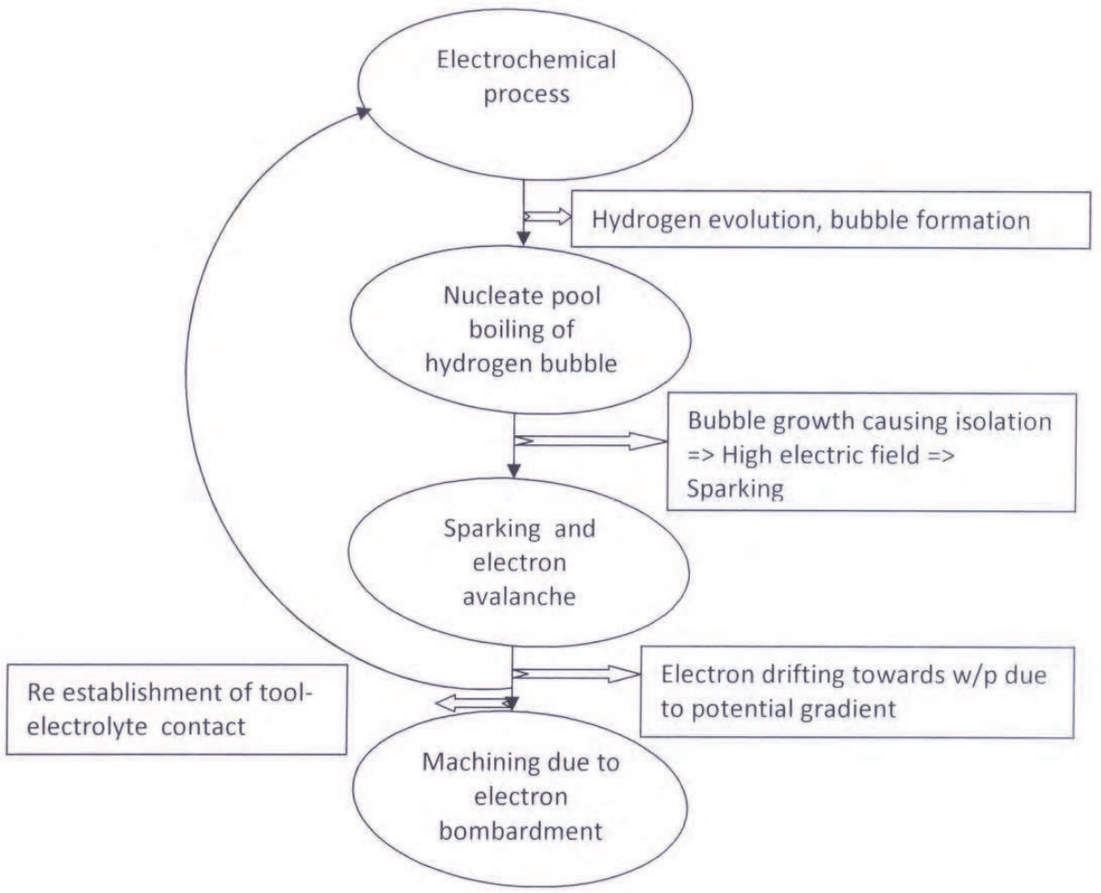

Fig. 9. Operational flow of ECSMM process showing intermediate processes.

It starts with the electron generation, these in turn generating the secondary electrons and hence causing the electron avalanche. These energetic electrons get drifted away from cathode (tool) to the work piece very quickly due to the high potential gradient getting generated within the tool – work piece gap because of the hydrogen bubble isolating the electrolyte, as described. These drifted electrons bombard on the work piece surface. A large current spike is seen as a result of electron flow from cathode to work piece as actually seen during the transient current measurements. The bombardment of electrons on the work piece surface results in intense heating and hence metal removal takes place.
The overall material mechanism of the ECSM process can be understood in the light of the electrochemistry, heat transfer, ionization theory and electrical response of the system. The operational flow of the overall process is as shown in Figure 9. Each involved intermediate process and the cross relation with other sub processes is illustrated further in section 5.1.1-5.1.4.

5.1.1 Electrochemical process

When the supply to the electrolyte cell is applied in the proper polarity, (i.e. positive terminal connected to anode and negative terminal to cathode) electrochemical action starts. electrons move from the cathode–electrolyte interface, and go to the solution. At the anode–electrolyte interface, equal number of electrons are discharged from the solution to the anode. Electrochemical reactions that occur at the electrode–electrolyte interface continuously supply electrons from cathode to solution and solution to anode. The type of reaction depends on the characteristics of electrodes, electrolyte and applied voltage. This is called as the 'migration' state of the ECSMM process.

a. Reactions at anode and electrolyte interface:

The electrochemical reactions at anode–electrolyte interface cause generation of oxygen gas. Dissolution of anode does not occur as the anode material used is graphite which is non consumable.

$$4(OH)^{-} \rightarrow 2H_2O + O_2 + 4e^{-}$$

b. Reactions at cathode and electrolyte interface:

Following electrochemical reactions take place at cathode–electrolyte interface, and cause evolution of hydrogen gas.

$$Cu^{2+} + 2e^{-} \rightarrow Cu$$

$$2H^{+} + 2e^{-} \rightarrow H_2\uparrow$$

$$Na^{+} + e^{-} \rightarrow Na$$

$$2Na + 2H_2O \rightarrow 2NaOH + H_2\uparrow$$

$$2H_2O + 2e^{-} \rightarrow H_2\uparrow + 2OH^{-}$$

Hydrogen gas evolves at the cathode, subsequently forming an isolating film, as depicted in Figure 8 a, or b, which leads to sparking across the bubbles between the cathode and electrolyte interface.

c. Reduction of electrolyte in the bulk:
It is given by:

$$NaOH \rightarrow Na+ + OH-$$

These liberated positive ions move towards cathode and negative ions move towards anode. In the external circuit, electrons move towards the cathode–electrolyte interface, and go to the solution. At the anode–electrolyte interface equal numbers of electrons are discharged from the solution to the anode. Electrochemical reactions that occur at the electrode–electrolyte interface continuously supply electrons from cathode to solution and solution to anode. This ionic and electronic current is the average current of the order of 100 – 200 mA.

5.1.2 Nucleate pool boiling of hydrogen bubble

The tip of the cathode gets heated up this causes nucleate pool boiling of hydrogen bubble that leads to development and formation of isolation vapor chamber of H_2 gas. The heat transfer controlled growth model applies and the radius of the bubble as a function of time can be found by the corresponding equations. According to this model, the vapor bubble starts growing till it reaches its departure diameter, reaching which the bubble gets detached from the lower surface of the tool. An isolating film of hydrogen gas bubble covers the cathode tip portion in the electrolyte, abruptly a large dynamic resistance is present and the current through the circuit becomes almost zero. At the same moment, a high electric field of the order of 10^7 V/m gets applied. This high electric field causes the bubble discharge, sparking takes place. This leads to generation of energetic electros. These electrons generate secondary electrons. These get drifted towards the workpiece surface due to potential gradient.

5.1.3 Sparking and electron avalanche

The high electric field causes spark within the gas bubble isolating the tip. The spark should occur between the tip of the tool and the inner surface of the electrolyte. At the instant when spark occurs, an avalanche of electrons caused by ionization flow towards work piece kept around 20 μm distance away from the tool tip. This avalanche of electron is manifested as the current pulses of short duration and high amplitude as seen in Figure 7a,b. As the potential gradient after varied varied, these electrons drift through the sparking channel towards the work piece surface. Experimentally it is found that this time to reach the electron avalanche to the work piece depends on the separation distance. This time is longer for work piece kept at a 500 μm distance (Kulkarni et al., 2002) than that kept at 20 μm. This fact supports that it is a drifting phenomena of the electron avalanche.

5.1.4 Material removal

The bombardment of electrons on the glass work piece surface results in intense heating and hence material removal takes place. Atoms of the parent material get dislodged and material removal takes place. There are partial sparks occurring, theses may not be having enough energy to cause the material removal. These hamper the efficiency of the process and also affect the surface finish.

At the same instant, the bubble geometry gets disturbed the contact between the tool and the electrolyte reestablishes. Electrochemical reaction takes over, bubble gets built up and the cycle keeps repeating itself. This makes the process discrete and repetitive.
All these intermediate processes described in sections 5.1 through 5.1.4 are correlated with the transient current pulses as observed in Figures 7 a and b. Figure 10 presents this correlation pictorially. The figure is self explanatory illustrating the time events during the ECSMM process w.r.t current.

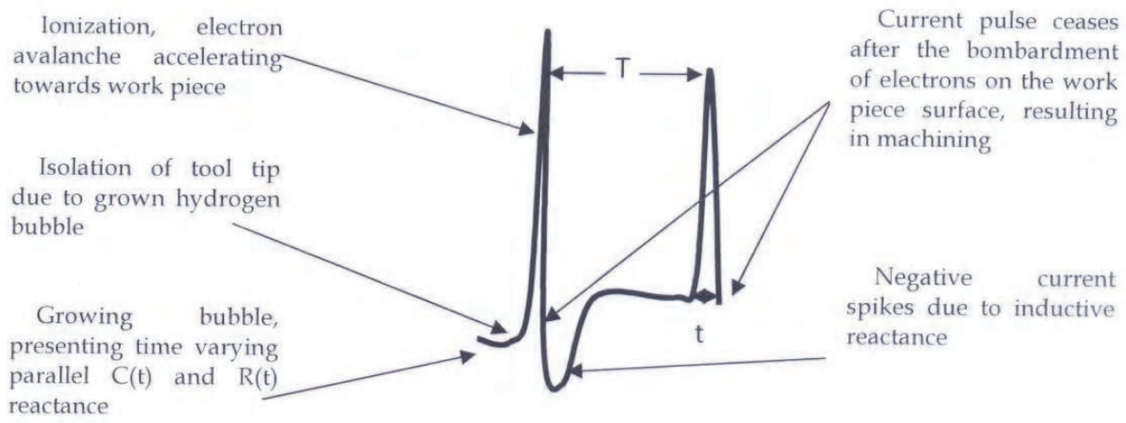

T: Time between two sparks, i.e. time required for the bubble growth till isolation of tool tip from electrolyte (T ranges between few hundreds of μs to few tens of ms)
t: Time required to reach the electron avalanche to the work piece surface
(t ranges between tens of μs to few hundreds of μs)
Sparking frequency $f_{sparking} = 1/(T+t)$
($f_{sparking}$ ranges between few hundred hertz to few tens of kHz)

Fig. 10. Part of an entire transient, instantaneous current pulse illustrating various time events during the ECSMM process w.r.t current

6. Concluding remarks

ECSMM process is found to be suitable for production of micro channels on glass pellets. The width of the micro channels achieved is in the range of 400 – 1100 μm. The depth achieved is in the range of 75 -120 μm. The time required to form these micro channels of 5mm length is about 5000 μm. SEM analysis shows that the micro machined surface is produced by melting and vaporization. The current pulses show the stochastic nature of the spark formation process.
The material removal mechanism is complex. It involves various intermediate processes such as: electrochemical reactions followed by nucleate pool boiling, followed by breakdown of hydrogen bubbles, generating the electrons, these electrons drifting towards the workpiece and causing the material removal. The process starts all over again by electrochemical reactions once the bubbles are burst due to sparking. And re establishment of contact between tool electrode – electrolyte takes place.

Close control for gap adjustment is must. Research efforts must be made to reduce the low energy sparks due to partial isolation to enhance the efficiency of the process and surface finish.

7. Acknowledgements

I am indebted to Prof. V K Jain for his immense guidance and support throughout my academic life at IIT Kanpur. I am thankful to Prof. K A Misra for his guidance in carrying out the work. Financial support for this work from Department of Science and Technology, Government of India, New Delhi, is gratefully acknowledged (Grant no. SR/S3/MERC-079/2004). Thanks are due to the staff at Manufacturing Science Lab and Centre for Mechatronics, at IIT, Kanpur. Ms. Shivani Saxena and Mr. Ankur Bajpai, Research Associates in the project, helped in carrying out the experiments. Their help is duly acknowledged. Thanks are also due to the staff at Glass Blowing section of IIT, Kanpur.

8. References

Basak, I. Ghosh, A. (1992). Mechanism of Material Removal in Electrochemical Discharge Machining: A Theoretic Model and Experimental Verification. J. Mater. Process. Technology, 71, 350–359

Basak, I., and Ghosh, A. (1996). Mechanism of Spark Generation During Electrochemical Discharge Machining: A Theoretical Model and Eexperimental Investigation. Jr. of Materials Processing Technology, 62 46-53

Bhattacharyya, B., Doloi, B. N., and Sorkhel, S. K. (1999). Experimental Investigation Into Electrochemical Discharge Machining of Non conductive Ceramic Material. Journal of Materials Processing Technology, 95, 145-154

Claire, L.C., Dumais, P., Blanchetiere, C., Ledderhof, C.J., and Noad, J.P., (2004). Micro channel arrays in borophsphosilicate Glass for Photonic Device and optical sensor applications, *Tokyo konfarensu Koen Yoshishu* L1351C, 294authors name missing

Coraci, A., Podarul, C., Maneal, E., Ciuciumis, A. and Corici, O. (2005). New technological surface micro fabrication methods used to obtain microchannels based systems onto various substrates', *Semiconductor Conference CAS 2005 Proceedings*, Vol. 1, pp.249–252

Crichton, I.M. and McGough, J.A. (1985). Studies of the discharge mechanisms in electrochemical arc machining', *J. of Appl. Electrochemistry*, Vol. l15, pp.113–119

Deepshikha, P. (2007). Generation of microchannels in ceramics (quartz) using electrochemical spark machining, MTech thesis, IIT Kanpur

Fascio, V., Wüthrich, R. and Bleuler, H. (2004). Spark assisted chemical engraving in the light of electrochemistry, *Electrochimica Acta*, Vol. 49, pp.3997–4003

Han, M-S., Min, B-K. and Lee, S.J. (2008). Modeling gas film formation in electrochemical discharge machining processes using a side-insulated electrode', *J. Micromech. Microeng*., doi: 10.1088/0960-1317/18/4/045019

Hnatovsky, C., Taylor, R.S., Simova, E., Rajeev, P.P., Rayner, D.M., Bhardwaj, V.R. and Corkum, P.B. (2006). Fabrication of micro channel in glass using focused femto second laser radiation and selective chemical etching', *Applied Physics*, Vol. 84, Nos. 1–2, pp.47–61

Jain, V.K., Dixit, P.M. and Pandey, P.M. (1999). On the analysis of electro chemical spark machining process', *Int. J. of Machine Tools and Manufacture*, Vol. 39, pp.165–186

Kulkarni, A. V., Jain, V.K. and Misra, K.A. (2011c). Application of Electrochemical Spark Process for Micromachining of Molybdenum, ICETME 2011, Thapar University, Patiala, Mr J S Saini, Mr Satish Kumar, Mr Devender Kumar, Eds., pp. 410-415.

Kulkarni, A. V., Jain, V.K. and Misra, K.A. (2011b). Electrochemical Spark Micromachining: Present Scenario, *IJAT* vol. 5, no. 1, pp. 52-59.

Kulkarni, A.V., Jain, V.K. and Misra, K.A. (2011a). Electrochemical spark micromachining (microchannels and microholes) of metals and non-metals, *Int. J. Manufacturing Technology and Management*, vol. 22, no. 2, 107-123.

Kulkarni A. V., Jain V. K., and Misra K. A., (2010c). Development of a Novel Technique to Measure Depth of Micro-channels: A Practical Approach for Surface Metrology, Proc. of the ICAME 2010, R. Venkat Rao, Ed, pp. 1008-1012.

Kulkarni A. V., Jain V. K., and Misra K. A., (2010b). Traveling Down the Microchannels: Fabrication and Analysis, AIM 2010, 978-1-4244-8030-2/10 ©2010 **IEEE,** pp. 1186-1190.

Kulkarni, A. V., V. K. Jain, V.K. and Misra, K.A. (2010a). Simultaneous Microchannel Formation and Copper Deposition on Silicon along with Surface Treatment, IEEM 2010 IEEE, DOI: 10.1109/IEEM.2010.5674509, pp 571-574.

Kulkarni, A. V. (2009). Systematic analysis of electrochemical discharge process, Int. J. Machining and Machinability of Materials, 6, ¾, pp 194-211.

Kulkarni, A. V., Jain, V. K., Misra, K. A. and Saxena P., (2008). Complex Shaped Micro-channel Fabrication using Electrochemical Spark, Proc. Of the 2nd International and 23rd AIMTDR Conf. Shanmugam and Ramesh Babu, Eds, pp. 653-658.

Kulkarni, A. V. Sharan and G.K. Lal, (2002). An Experimental Study of Discharge Mechanism in Electrochemical Discharge Machining, International Journal of Machine Tools and Manufacture, Vol. 42, Issue 10, pp. 1121-1127.

Kulkarni, A. V. (2000). An experimental study of discharge mechanism in ECDM, M.Tech. Thesis, IIT Kanpur, Kanpur, India.

Marc Madou, (1997). Fundamentals of micro fabrication, *CRC Press*

Rajaraman, S., Noh, H-S., Hesketh, P.J. and Gottfried, D.S. (2006) 'Rapid, low cost micro fabrication technologies toward realization of devices for electrophoretic manipulation', *Sensors and Actuators B*, Vol. 114, pp.392–401

Rodriguez, I., Spicar-Mihalic, P., Kuyper, C.L., Fiorini, G.S. and Chiu, D.T. (2003) 'Rapid prototyping of glass materials', *Analytica Chimica Acta*, Vol. 496, pp.205–215.

Sorkhel, S.K., Bhattacharyya, B., Mitra, S. and Doloi, B. (1996) 'Development of electrochemical discharge machining technology for machining of advanced ceramics', *International Conference on Agile Manufacturing*, pp.98–103

Wuthrich, R., Fascio, V., Viquerat, D. and Langen, H. (1999) 'In situ measurement and micromachining of glass', *Int. Symposium on Micromechatronic and Human Science*, pp.185–191

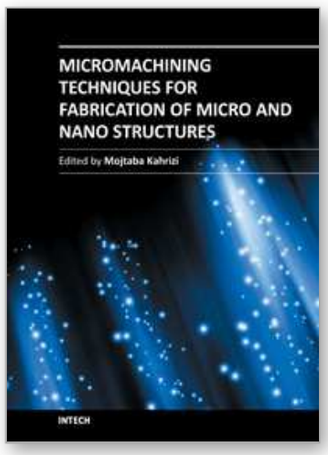

Micromachining Techniques for Fabrication of Micro and Nano Structures

Edited by Dr. Mojtaba Kahrizi

ISBN 978-953-307-906-6
Hard cover, 300 pages
Publisher InTech
Published online 03, February, 2012
Published in print edition February, 2012

Micromachining is used to fabricate three-dimensional microstructures and it is the foundation of a technology called Micro-Electro-Mechanical-Systems (MEMS). Bulk micromachining and surface micromachining are two major categories (among others) in this field. This book presents advances in micromachining technology. For this, we have gathered review articles related to various techniques and methods of micro/nano fabrications, like focused ion beams, laser ablation, and several other specialized techniques, from esteemed researchers and scientists around the world. Each chapter gives a complete description of a specific micromachining method, design, associate analytical works, experimental set-up, and the final fabricated devices, followed by many references related to this field of research available in other literature. Due to the multidisciplinary nature of this technology, the collection of articles presented here can be used by scientists and researchers in the disciplines of engineering, materials sciences, physics, and chemistry.

InTech Europe
University Campus STeP Ri
Slavka Krautzeka 83/A
51000 Rijeka, Croatia
Phone: +385 (51) 770 447
Fax: +385 (51) 686 166
www.intechopen.com

InTech China
Unit 405, Office Block, Hotel Equatorial Shanghai
No.65, Yan An Road (West), Shanghai, 200040, China
中国上海市延安西路65号上海国际贵都大饭店办公楼405单元
Phone: +86-21-62489820
Fax: +86-21-62489821

IntechOpen